Evaluation of CMPA precipitation estimate in the evolution of typhoon-related storm rainfall in Guangdong, China

Dashan Wang, Xianwei Wang, Lin Liu, Dagang Wang, Huabing Huang and Cuilin Pan

ABSTRACT

The merged precipitation data of Climate Prediction Center Morphing Technique and gauge observations (CMPA) generated for continental China has relatively high spatial and temporal resolution (hourly and 0.1°), while few studies have applied it to investigate the typhoon-related extreme rainfall. This study evaluates the CMPA estimate in quantifying the typhoon-related extreme rainfall using a dense rain gauge network in Guangdong Province, China. The results show that the event-total precipitation from CMPA is generally in agreement with gauges by relative bias (RB) of 2.62, 10.74 and 0.63% and correlation coefficients (CCs) of 0.76, 0.86 and 0.91 for typhoon Utor, Usagi and Linfa events, respectively. At the hourly scale, CMPA underestimates the occurrence of light rain (<1 mm/h) and heavy rain (>16 mm/h), while overestimates the occurrence of moderate rain. CMPA shows high probability of detection (POD = 0.93), relatively large false alarm ratio (FAR = 0.22) and small missing ratio (0.07). CMPA captures the spatial patterns of typhoon-related rain depth, and is in agreement with the spatiotemporal evolution of hourly gauge observations by CC from 0.93 to 0.99. In addition, cautiousness should be taken when applying it in hydrologic modeling for flooding forecasting since CMPA underestimates heavy rain (>16 mm/h).

Key words | CMPA, evaluation, extreme rainfall, typhoon

Dashan Wang
Xianwei Wang
Lin Liu
Dagang Wang
Huabing Huang
Cuilin Pan
Center of Integrated Geographic Information Analysis, School of Geography and Planning, and Guangdong Key Laboratory for Urbanization and Geo-simulation,
Sun Yat-sen University,
Guangzhou,
China

Lin Liu (corresponding author)
Department of Geography,
University of Cincinnati,
Cincinnati,
OH,
USA
E-mail: *liulin2@mail.sysu.edu.cn*

INTRODUCTION

Extreme precipitation often causes or induces flooding, landslides, and mudslides (Hong *et al.* 2006; Wu *et al.* 2012). Heavy rainfall driven by tropical cyclones (also called typhoons) frequently cause casualties and enormous property losses in coastal areas (Negri *et al.* 2005). For example, Katrina struck the Gulf Coast of Florida, Alabama, Mississippi and Louisiana on August 2005 (Knabb *et al.* 2005), Morakot hit Taiwan and Fujian Provinces of China on August 2009 (Van Nguyen & Chen 2011), and Yasi hit the Queensland coast of Australia on February 2011 (Chen *et al.* 2013d). All brought huge amounts of rainfall and caused heavy casualties and serious economic losses.

Accurate measurement of precipitation with fine resolution and reasonable accuracy is essential but challenging (Li *et al.* 2013). Automatic rain gauge networks can provide near-real time measurements, while the representativeness of a sparse and uneven distribution of gauges is worthy of consideration (Li & Shao 2010). Weather radar is capable of monitoring local precipitation under fine spatial resolution and reliable quality, although it is affected by atmospheric conditions and high terrain in mountainous areas (Zhang *et al.* 2011a). With the development of satellite precipitation retrievals, high resolution and multi-sensor precipitation products come out in succession and are available in near-real

doi: 10.2166/hydro.2016.241

time, such as PERSIANN (hourly and 0.04°; Sorooshian *et al.* 2000), the US NOAA CPC Morphing Technique (CMORPH) (30 minutes and 8 km; Joyce *et al.* 2004), Naval Research Laboratory (NRL)-Blend (3 hours and 0.25°; Turk & Miller 2005), the Tropical Rainfall Measuring Mission (TRMM) Multi-satellite Precipitation Analysis (TMPA, 3 hours and 0.25°; Huffman *et al.* 2007), and the Global Precipitation Measurement products (4 km and 30 minutes; Sorooshian *et al.* 2011). For continental China, version 1.0 of the merged precipitation data of the Climate Prediction Center Morphing Technique and gauge based precipitation (CMPA, 0.1° and 1 hour) are available for recent years and demonstrate high agreements with ground observations (Shen *et al.* 2014). These products greatly improve hydrological simulation and flood prediction due to their large coverage and relatively high spatial resolution (Anagnostou 2004; Hossain & Lettenmaier 2006; Behrangi *et al.* 2011; Jiang *et al.* 2012).

Satellite precipitation estimates have considerable importance in many hydrological and meteorological applications (Tian *et al.* 2007). The satellite-based precipitation products usually need verification before being applied in hydrologic modeling (Turk *et al.* 2008). The comprehensive evaluation to satellite precipitation products has significant implications. On the one hand, the knowledge of error characteristics is beneficial to the improvement of retrieval algorithm (Dinku *et al.* 2011). On the other hand, the error characteristics offer suggestions on how the data are properly used in hydrologic and climatic models since errors may vary notably among different seasons and climate settings (Dai *et al.* 2007; Zhou *et al.* 2008; Stampoulis & Anagnostou 2012). Satellite precipitation estimates, after bias adjustment, can provide better performance in hydrological modeling (Su *et al.* 2008; Yong *et al.* 2010).

The current satellite rainfall estimates have limitations in detecting extreme rainfall but with great potential. For instance, the four products of TMPA 3B42 V6, 3B42 RT, PERSIANN-CCS and CMORPH greatly underestimates the peak rain rate for the extreme rainfall brought by the Typhoon Morakot in Taiwan and Fujian Provinces, China (Chen *et al.* 2013a). Both TMPA 3B42 V6 and CMORPH considerably underestimates the moderate and heavy rainfall and overestimates the light rainfall of typhoon-related precipitation over mainland China (Yu *et al.* 2009). The TMPA 3B42 V7 performs better over ocean than over land, and underestimates the frequency of heavy rain over land according to the assessment study using PACRIAN rain gauges over low-lying atolls and coastal islands in the tropical Pacific basins (Chen *et al.* 2013e). Meanwhile, Habib *et al.* (2009) highlight the potential of TMPA products and demonstrate the significant improvement from the real-time version to the research version in a study using six tropical-related heavy rainfall events in Louisiana, USA. Prat & Nelson (2013) quantify the contribution of tropical-related rainfall over land to the annual rainfall around the world using TMPA 3B42 V7 estimate, and this contribution could be better quantified if the underestimate of peak rain rate of TMPA is adjusted. In addition, the emergence of CMPA estimate has not received enough attention, although it shows high agreements with ground observations (Shen *et al.* 2014) and is used in a few studies (Yu & Liu 2015; Chen *et al.* 2015, 2016). Moreover, few studies use the CMPA to quantitatively analyze the typhoon-related heavy rainfall in China.

Therefore, the primary objective of this study is to evaluate the performance of the hourly CMPA product on typhoon-related storms using an independent, dense rain gauge network in Guangdong Province, China. Seven typhoon-related storm events were selected to compare the CMPA estimates with dense gauge recordings over 1,330 stations. This study intends to investigate the error characteristics of the CMPA estimate on typhoon storms through comprehensive assessment, such as quantifying total rain depth, rainfall hyetograph, spatiotemporal pattern and storm evolutions, and so on.

STUDY AREA AND DATA

Study area

The study area is in the Guangdong Province of southern China, which contains 21 prefecture-level cities/regions and spans 20–26 °N in latitude and 109–118 °E in longitude (Figure 1). It is in sub-tropic and tropic climate settings controlled mainly by the South China Sea Monsoon (Yang *et al.* 2015). The annual mean air temperature and rain depth are 22 °C and 1,800 mm, respectively (Zeng *et al.* 2014). The wet season normally ranges from April to September. Typhoon-related heavy rain events occur in the late wet season from July to September and even occasionally in October (Wang

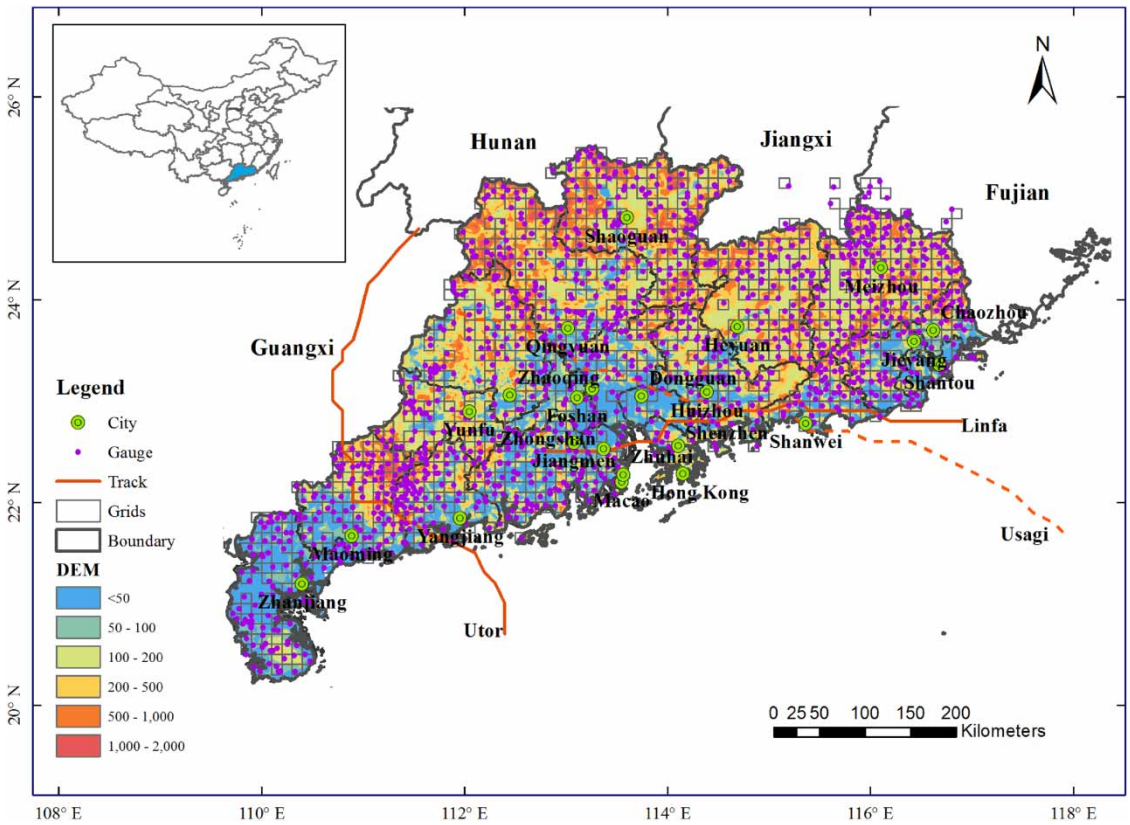

Figure 1 | Terrain of Guangdong Province, China, CMPA grids (grey squares), rain gauges (purple dots) and the tracks of three typhoon events (Utor, Usagi and Linfa). Please refer to the online version of this paper to see this figure in color: http://dx.doi.org/10.2166/hydro.2016.241 (open access).

et al. 2015). On average, 2.8 typhoons have struck this area in recent years and contributed 20–30% to the annual rain depth (Ren *et al.* 2006). The low-lying coastal terrains and the mountainous areas are susceptible to typhoon-induced floods (Zhang *et al.* 2011b). In addition, the permanent residents of Guangdong Province totalled 104 million in 2010, and the Gross Domestic Product reached 4,600 billion Yuan, accounting for 11.4% of the national total (Wang *et al.* 2013a). The rapidly growing population and dramatically flourishing economics make this area more vulnerable to flooding events.

Typhoon events

There were a total of seven typhoon events which made landfall in Guangdong Province from 2013 to 2015 (Table 1). Three typhoon rainfall events of Utor, Usagi and Linfa (Figure 1) had

Table 1 | Basic information for the seven typhoon rainfall events

Event name	Start time (UTC)	End time (UTC)	Period (hour)	Spatial mean rain depth (mm)	Affected gauges	CMPA grids
Utor	2013-8-14-00	2013-8-16-12	60	175	972	708
Usagi	2013-9-22-00	2013-9-23-12	36	68	1,158	836
Linfa	2015-7-9-00	2015-7-10-12	36	48	1,070	785
Mujigae	2015-10-3-18	2015-10-5-10	40	179	626	440
Kalmaegi	2014-9-15-08	2014-9-16-20	36	103	477	328
Rammasun	2014-7-18-06	2014-7-19-06	24	59	451	314
Rumbia	2013-7-1-14	2013-7-2-06	16	33	567	403

a wider impact on the entire Guangdong Province than the other four typhoons of Mujigae, Kalmaegi, Rammasun and Rumbia (Figure A1, available with the online version of this paper), and are presented in the main text. The results for the other four typhoons are provided in the auxiliary material and cited in the text with capital letter of A, e.g. Figure A1.

Typhoon Utor was a long-lived storm, which originated as a tropical disturbance in the west Pacific on August 8 and became a super typhoon on 10 August. After passing through the Philippines, Utor strengthened again and landed on Yangjiang at 7:50 UTC on August 14, 2013, with a peak wind speed of 42 m/s, then moved northward and eventually dissipated on August 18, 2013 (Figure 1). It is one of the most extreme typhoon rainfall events in Guangdong Province in the last 50 years, causing 1.33 billion Yuan property loss and 84 people dead or missing (AOF 2014). The average rainfall in Guangdong is more than 170 mm (Table 1).

Typhoon Usagi is one of the strongest typhoons that has landed on east Guangdong in the last 40 years. It landed on Shanwei at 11:40 UTC on September 22, 2013 with a peak wind speed of 45 m/s, and moved northwest across Guangdong before dissipating in the morning of September 23, 2013 (Figure 1). Typhoon Usagi brought strong winds and high tide surges (1.63 m at Zhelang station), 100–200 mm of rain to most areas of Guangdong Province (Table 1), caused 5.86 billion Yuan property loss and affected five million people with 30 people dead (AOF 2014).

Typhoon Linfa became a typhoon at 12:00 UTC on July 8, 2015 in the northeast of the South China Sea. It landed on Shanwei at 04:15 UTC on July 9, 2015 with a peak wind speed of 35 m/s (Figure 1). It then moved westward and brought an average of 48 mm of rain to east Guangdong Province (Table 1).

Typhoon Mujigae originated as a tropical disturbance in the South China Sea and moved toward the northwest. It made landfall near Zhanjiang City, Guangdong Province at 5:00 UTC on October 4, 2015 with a peak wind speed of 50 m/s, and then dissipated 22 h later (Figure A1(a)). It brought 100–200 mm rainfall to the western and central areas of Guangdong Province (Table 1).

Typhoon Kalmaegi developed on September 12, 2014 as a tropical depression in the west Pacific. It later made landfall on northeast Philippines at 11:00 UTC on September 14. After crossing the South China Sea, Kalmaegi strengthened again and landed on Hainan Island and Zhanjiang City successively in the morning of September 16, with a peak wind speed of 40 m/s (Figure A1(a)). It brought an average of 103 mm of rain to southwestern Guangdong Province (Table 1).

Typhoon Rammasun was a long-lived storm, which originated in the west Pacific on July 12, 2014, and then moved westward. After crossing the Philippines, Rammasun took a northwest turn and passed the South China Sea. It strengthened and landed on Zhanjiang at 11:00 UTC on July 18, 2014, with a peak wind speed of 60 m/s. It dissipated on July 20, 8 days after its original development (Figure A1(c)). It brought an average of 59 mm of rain to the western areas of Guangdong Province (Table 1).

Typhoon Rumbia became a typhoon at 02:00 UTC on July 1, 2013 in the central South China Sea. It landed on Zhanjiang at 21:30 UTC on July 1 with a peak wind speed of 30 m/s (Figure A1(d)). Then it moved northward and brought nearly 100 mm of rain to the Leizhou Peninsula of Guangdong Province (Table 1).

Gauge data

The dense rain gauge network is maintained by the Department of Water Resources in Guangdong Province (www.gdwater.gov.cn/). All rain depth data are accumulated hourly with a precision of 0.1 mm, and the temporal coverage starts from October 2012 to present. There are over 1,330 stations with valid rain depth recorded for the seven typhoon-related storm events from 2013 to 2015. To our best knowledge, these gauge observations were not incorporated in the interpolation process of the CMPA estimate. It is rational and significant to validate the CMPA estimates using rain depth data from the stations in this study.

CMPA

The CMPA data are merged hourly precipitation products with $0.1 \times 0.1^{\circ}$ spatial resolution (Shen *et al.* 2014; http://cdc.nmic.cn/home.do) and are available from 2008 to present. The merging process is as follows: (1) the hourly precipitation measurements from more than 30,000 automatic weather stations over China are interpolated into

$0.1 \times 0.1^{\circ}$ grids; (2) the 8 km CMORPH precipitation estimates (Joyce *et al.* 2004) every 30 minutes are summed into hourly accumulation and re-sampled into $0.1 \times 0.1^{\circ}$ grids; (3) the re-sampled CMORPH data are adjusted to correct biases by using the probability density function based on gauge measurements; (4) the final hourly $0.1 \times 0.1^{\circ}$ products are generated by merging the adjusted CMORPH data with the gauge data using the improved optimum interpolation technique. The corresponding root mean squared difference (RMSD) and correlation coefficient (CC) are 0.6 mm/hour and 0.8, respectively (Shen *et al.* 2014).

METHODOLOGY

Normal comparisons

The typhoon-affected rainfall is first defined according to the trajectories of typhoon centers before carrying out the normal comparison and other evaluations. The time and trajectories of the typhoon events were retrieved from the Department of Water Resources in Guangdong Province. Rainfall observed within a radius of 400 km from the typhoon center is treated as typhoon-related rainfall in this area, while a 500-km radius is applied in the northwest of Australia (Lonfat *et al.* 2004; Dare *et al.* 2012). If the distance of a rain gauge from the typhoon center during any hour is less than 400 km, that particular hour of that gauge is defined as a 'typhoon hour'. The typhoon-related storms normally last more than 24 hours (Table 1). Only those gauges with at least 12 typhoon hours are used in the following evaluation. The 12 hours represent a range of roughly 300 km since the mean moving speed of typhoon after landfall is 20–25 km/h. In practice, gauges with less than 12 typhoon hours usually have much less rainfall and are less affected by the typhoon event than those with over 12 typhoon hours.

The common grid-to-point comparison method is utilized in comparing the grid data of CMPA ($0.1 \times 0.1^{\circ}$) to the point gauge observations (Li *et al.* 2013). To reduce the scale errors, only those grids that contain at least one gauge are extracted for further evaluation. The mean value of all gauge measurements within a single grid is adopted if there is more than one gauge in a CMPA grid (Yong *et al.* 2010, 2014). Rain or no-rain hour is defined by a threshold of 0.1 mm/h. The total number of the affected gauges and grids are listed in Table 1.

Three normal comparison indices, CC, relative bias (RB) and RMSD, are adopted for the evaluation. They are defined in Equations (1)–(3) (Yong *et al.* 2010):

$$\mathrm{CC} = \frac{\sum_{i=1}^{n}(G_i - \bar{G})(M_i - \bar{M})}{\sqrt{\sum_{i=1}^{n}(G_i - \bar{G})^2}\sqrt{\sum_{i=1}^{n}(M_i - \bar{M})^2}} \tag{1}$$

$$\mathrm{RB} = \frac{\sum_{i=1}^{n}(M_i - G_i)}{\sum_{i=1}^{n} G_i} * 100\% \tag{2}$$

$$\mathrm{RMSD} = \sqrt{\frac{1}{n}\sum_{i=1}^{n}(M_i - G_i)^2} \tag{3}$$

where n is the number of gauges; G and M are the gauge observations and CMPA estimates, respectively.

The positive bias and negative bias will be offset in RB, which is used to describe the accumulative bias of the CMPA estimate. The standard mean bias is measured by RMSD. RB, RMSD and CC are used together to compare the CMPA estimate with rain gauge observations in this study and are also widely used in the radar and satellite rainfall validations (Yong *et al.* 2010; Jiang *et al.* 2012; Wang *et al.* 2013b; Shen *et al.* 2014).

Contingency statistics

Two contingency statistics, probability of detection (POD) and false alarm ratio (FAR), are used to measure the accuracy between CMPA and gauge observations. Each pair of hourly rainfall records from gauges and CMPA grids are classified as a Hit, Miss, or False (Table 2). Both POD and FAR are computed based on the count definition of Hit, Miss and False by Equations (4) and (5) (Ebert *et al.* 2007):

$$\mathrm{POD} = \frac{N_{hit}}{N_{hit} + N_{miss}} \tag{4}$$

$$\mathrm{FAR} = \frac{N_{false}}{N_{hit} + N_{false}} \tag{5}$$

Table 2 | Contingency table for gauge and CMPA estimate ($P_0 = 0.1$ mm/h)

	Gauge $\geq P_0$	Gauge $< P_0$
CMPA $\geq P_0$	Hit	False
CMPA $< P_0$	Miss	Null

where N_{hit} is the total count of hours when both gauge and CMPA observe rain, which is equal or larger than the rain rate threshold ($P_0 = 0.1$ mm/h). N_{miss} is the total count of hours when CMPA misses rain that is detected by the gauge. N_{false} is the total count of hours when CMPA detects rain that is not detected by the gauge.

POD shows how often the observed rain events are correctly detected by CMPA. FAR indicates the ratio of false alarm of CMPA. The perfect values of POD and FAR are 1 and 0, respectively.

Probability distribution functions

Probability distribution functions (PDFs) provide detailed information on the distribution of rainfall frequency and accumulated volume as a function of rain rate (Chen *et al.* 2013c). The probability distribution function by occurrence (PDFc) is the ratio of the rain hours within a rain rate interval to the total rain hours. The probability distribution function by volume (PDFv) is the ratio of the rain depth within each rain rate interval to the event-total rain depth. PDFc and PDFv are computed using the 'Hit' pairs of gauges and CMPA grids in Table 3.

K-means cluster analysis

The K-means cluster algorithm has been applied to characterize temporal patterns of rainfall in mainland China (Yin *et al.* 2014), Taiwan (Yu *et al.* 2014), and South Korea (Lee *et al.* 2012). It sets initial centers and calculates the minimum squared distance from the samples to its centers iteratively. Finally, all gauges are classified into three clusters (hyetograph types) by the K-means cluster analysis (Hartigan & Wong 1979) using the time series of hourly gauge observations for each rain event in this study. The three clusters are considered as the three parts of typhoon-related storms, the eyewall, the rainband and the outer rainband (Lonfat *et al.* 2004). The three hyetograph types for each event form a spatial pattern that corresponds to the three stages of the storm evolution, the initial landfall (storm center), advance and the dissipation. The according CMPA grids' values are extracted to compare with the gauge observations within each type or area for the seven storms.

Table 3 | Contingency statistics of the CMPA estimate versus gauge measurements for the seven typhoon rain events

Statistics		N_{hit}	N_{miss}	N_{false}	POD	FAR
Utor	All gauges	25,288	1,671	6,530	0.94	0.21
	Dist: ≤100 km	9,584	484	1,957	0.95	0.17
	Dist: 100–400 km	15,704	1,187	4,573	0.93	0.23
Usagi	All gauges	13,522	999	4,585	0.93	0.25
	Dist: ≤100 km	7,066	411	2,332	0.95	0.25
	Dist: 100–400 km	6,456	588	2,253	0.92	0.26
Linfa	All gauges	8,495	769	2,056	0.92	0.20
	Dist: ≤100 km	4,163	337	959	0.93	0.19
	Dist: 100–400 km	4,332	432	1,097	0.91	0.20
Mujigae	All gauges	12,461	387	2,275	0.97	0.15
	Dist: ≤100 km	1,940	135	833	0.93	0.30
	Dist: 100–400 km	10,521	252	1,442	0.98	0.12
Kalmaegi	All gauges	6,022	542	1,919	0.92	0.24
	Dist: ≤100 km	576	83	260	0.87	0.31
	Dist: 100–400 km	5,446	459	1,659	0.92	0.23
Rammasun	All gauges	3,443	404	1,298	0.90	0.27
	Dist: ≤100 km	793	19	243	0.98	0.23
	Dist: 100–400 km	2,650	385	1,055	0.87	0.28
Rumbia	All gauges	2,825	300	1,004	0.90	0.26
	Dist: ≤100 km	956	50	145	0.95	0.13
	Dist: 100–400 km	1,869	250	859	0.88	0.31

Gauges are separated according to their distance to the typhoon center track: ≤100 km and 100–400 km (POD: probability of detection; FAR: false alarm ratio).

RESULTS AND DISCUSSION

Events total rainfall

The event total precipitation from gauges and CMPA for the three events of Utor, Usagi and Linfa are illustrated in Figure 2. CMPA captures the overall patterns of the typhoon-related rainfall (Figure 2(d)–2(f)); in contrast, the gauges only show those within the administration boundary of Guangdong Province (Figure 2(a)–2(c)). For those gauge-CMPA grids (Figure 2(g)–2(i)), CMPA slightly overestimates the total rainfall by 2.62 (RB), 10.74 and 0.63% for the three events,

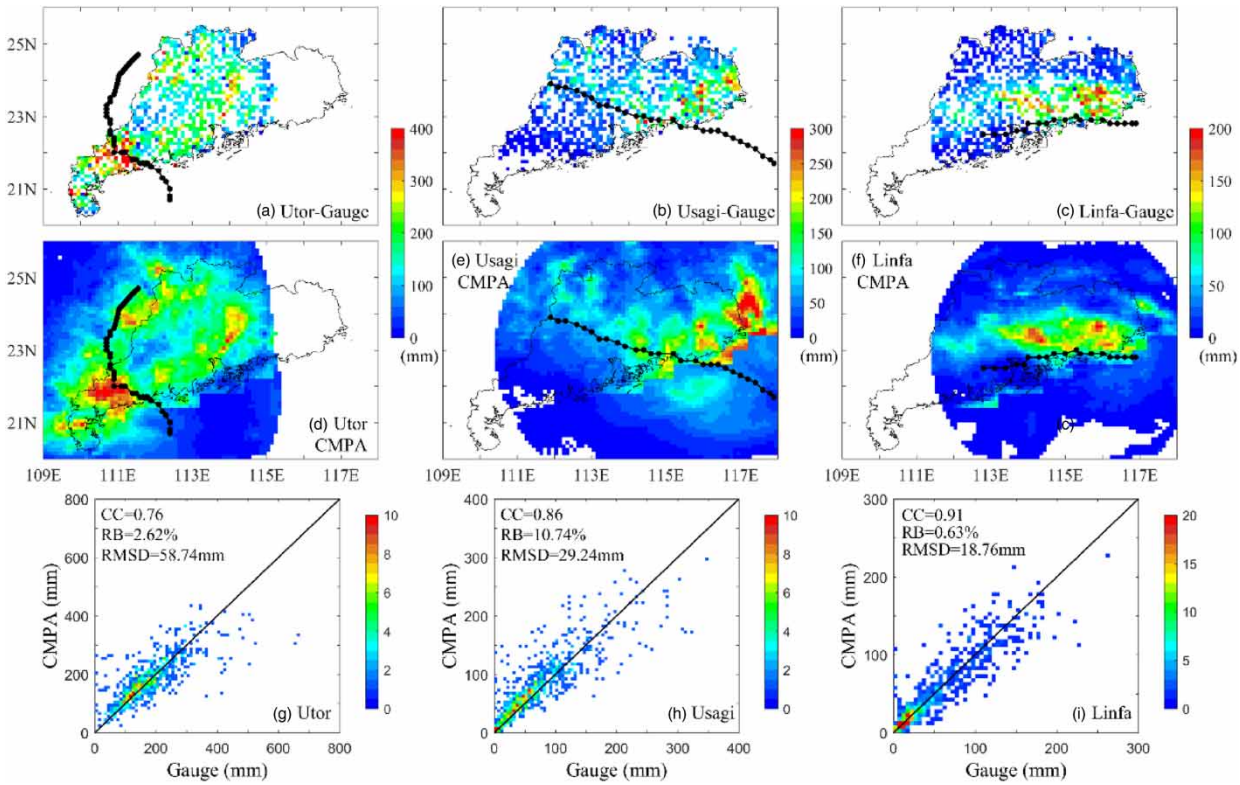

Figure 2 | Total precipitation for the three typhoon events (Utor, Usagi and Linfa) detected by rain gauges (a)–(c) and by CMPA (d)–(f), and the density-color scatter plots of CMPA versus gauge data (g)–(i). Density is the number of grids within a rain depth interval of 5 mm. The black lines in (a)–(f) outline the tracks of the three typhoon events.

respectively. The overall correlation coefficients (CC = 0.76, 0.86 and 0.91) are much higher than other satellite precipitation products (Habib *et al.* 2009; Huang *et al.* 2013), and are comparable to the radar rainfall estimate (Wang *et al.* 2008, 2013b). The results for the other four events of Mujigae, Kalmaegi, Rammasun and Rumbia are provided in the auxiliary material and show a similar pattern with those of the three events (Figure A1). Thus, CMPA is better applied to drive a hydrologic model for flooding forecasting for those watersheds crossing the administration boundary.

Typhoon Utor landed on Yangjiang and brought intense rain to the west of the typhoon centers, forming a storm center in Maoming and with a peak rain depth over 400 mm (Figure 2(a), 2(d) and 2(g)). Then, the rain belt moved along the east of the typhoon track. Another rain belt was in the far east of the track. CMPA captures the storm centers and rain belts as gauges do, but has better spatial coverage and details.

Typhoon Usagi landed on Shanwei and brought intense rain along the coast areas from Huizhou, Shanwei and Shantou to the southern Fujian Province (Figure 2(b), 2(e) and 2(h)). Different from the Utor, the storm center is about 250 km to the northeast of the typhoon track and in the Hanjiang Watershed, which is administered together by Guangdong and Fujian Provinces. Beneficial to the larger spatial coverage, CMPA better captures the storm center than the gauges from Guangdong Province. Usagi continued to move northwest across Guangdong and formed a light rain belt in the north of the track.

Typhoon Linfa also landed on Shanwei and moved westward (Figure 2(c), 2(f) and 2(i)). It brought intense rain of 100–200 mm in the north along the track, forming two storm centers in Jieyang and Huizhou, respectively. CMPA works best for this event by CC = 0.91, RB = 0.63% and RMSE = 18.76 mm.

Hourly gauge-CMPA comparison

The spatial distributions of CC, RB and RMSD reveal error characteristics of the hourly CMPA estimate in different

regions (Figure 3 and Figure A2 (available with the online version of this paper)). Overall, CMPA underestimates the rain depth in the storm centers and in the mountainous areas of Southwest Yunfu (Figure 3(d)–3(f) and Figure A2(e)–A2(h)) and has consistent CCs with gauge observations in different areas (Figure 3(a)–3(c) and Figure A2(a)–A2(d)). The distribution of RMSD also shows similar spatial patterns with the total precipitation for all three events and have large standard errors in the storm centers (Figure 3(g)–3(i) and Figure A2(i)–A2(l)). For the three events Utor, Usagi and Linfa, the ratio of positive RB are 60, 69 and 51%, and the mean RB are 5.76 ± 26.30, 13.15 ± 33.10 and 3.15 ± 33.82%, respectively. CMPA at the hourly scale also overestimates the light rain and underestimates the heavy rain (Figure 3(j)–3(l) and Figure A2(m)–A2(p)), which is a common challenge in correctly detecting heavy rain for satellites, radar or reanalysis data, such as in TRMM 3B42 (Chen *et al.* 2013b, 2013c; Prakash *et al.* 2015), TRMM PR (Rasmussen *et al.* 2013), Next generation weather Radar (NEXRAD) (Wang *et al.* 2008, 2013b) and ERA-Interim (Peña-Arancibia *et al.* 2013). CMPA demonstrates higher CC for Linfa than that for Usagi and Utor, similar

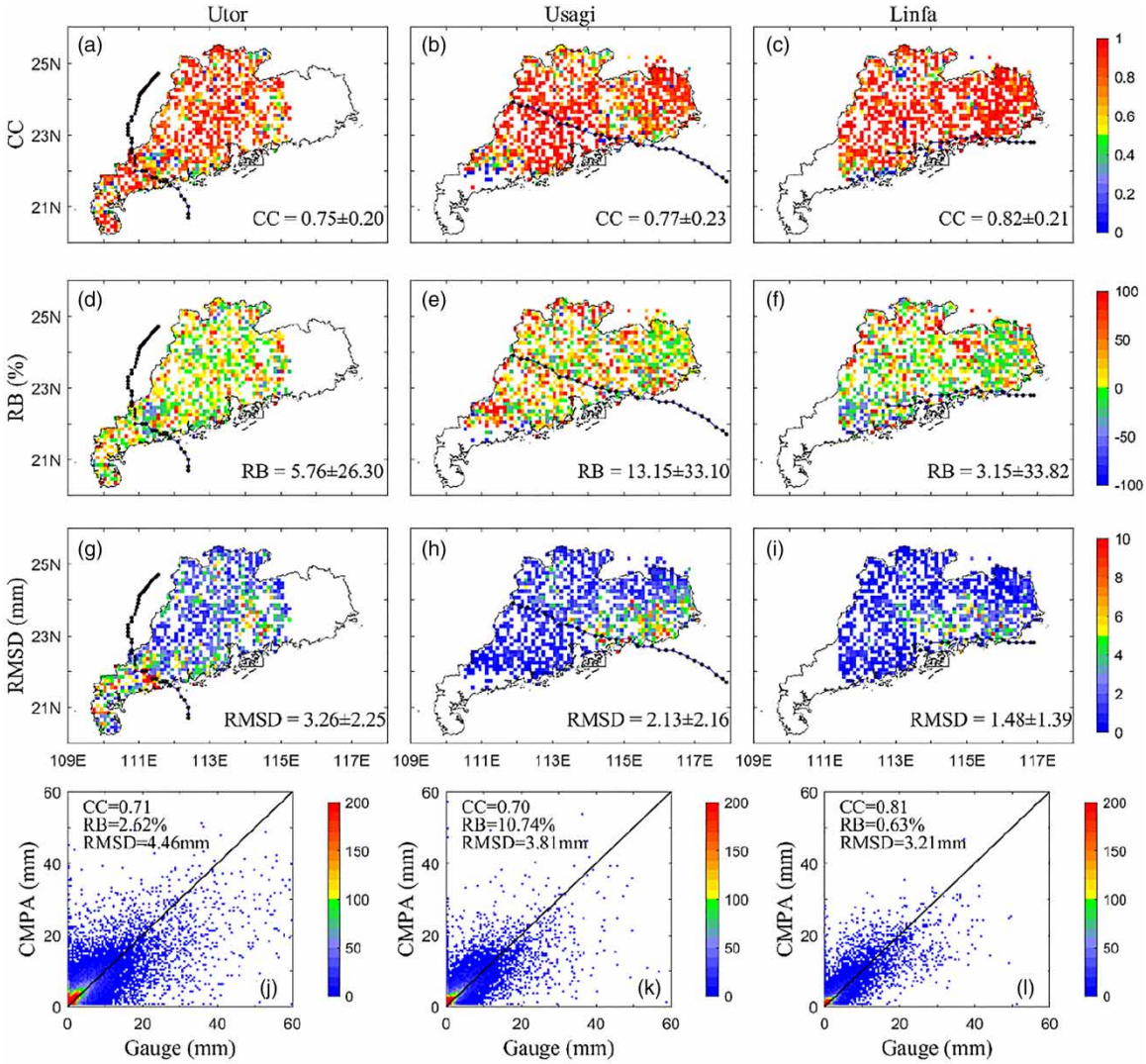

Figure 3 | Spatial distributions of the CC (a)–(c), RB (d)–(f), root mean square difference (g)–(i) and the density scatter plots (j)–(l) of the hourly CMPA estimates against rain gauge observations for the three typhoon rain events. All are computed using the gauge-CMPA pairs at each grid during the events. The black lines outline the tracks of typhoon events.

to the event total in Figure 2(g)–2(i). Chen *et al.* (2013d, 2013e) found that TMPA 3B42 performs better at lower elevation and in coastal areas in Australia, and these performance patterns do not evidently exist with the CMPA estimate in Guangdong Province.

CMPA has lower values of PDFc than gauges when the rain rate is less than 1 mm/h or larger than 16 mm/h for the three events (Figure 4 and Figure A3 (available with the online version of this paper)). Meanwhile, CMPA shows considerably good agreement with gauge observations for rainfall between 2 and 16 mm/h and has a positive RB for light rain and negative RB for heavy rain (Figure 5 and Figure A4 (available with the online version of this paper)). This indicates that CMPA misses the occurrence of light rain (<1 mm/h) remarkably and overestimates the occurrence of moderate rain between 2 and 16 mm/h, which is also partially attributed to the contribution of CMPA's overestimate to light rain and underestimate to heavy rain. Consequently, the PDFv of CMPA is smaller than that of gauges when the rain rate is smaller than 1 mm/h or larger than 16 mm/h for Utor, Usagi and Linfa. The PDFs of CMPA is in an inverse pattern to the daily TRMM 3B42 V6 and V7 over China and continental United States (Chen *et al.* 2013b, 2013c).

Contingency statistics

CMPA show similar high POD in all three events, while CMPA grids close to the typhoon center track have slightly higher values except for Mujigae and Kalmaegi (Table 3). In spite of the high POD, the false count is not negligible, and

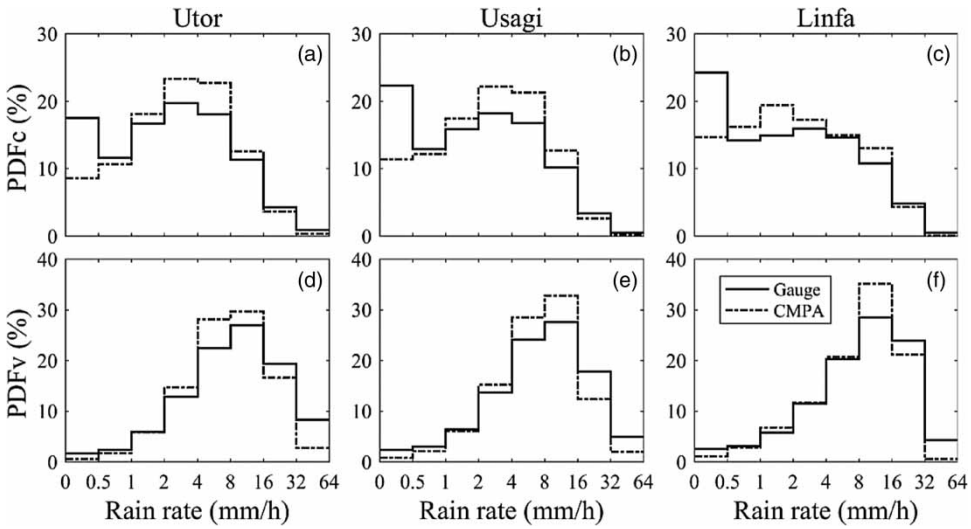

Figure 4 | (a)–(c) Probability distribution functions by occurrence (PDFc) and (d)–(f) by volume (PDFv) within different rain depth intervals for the hit pairs of the three typhoon rain events.

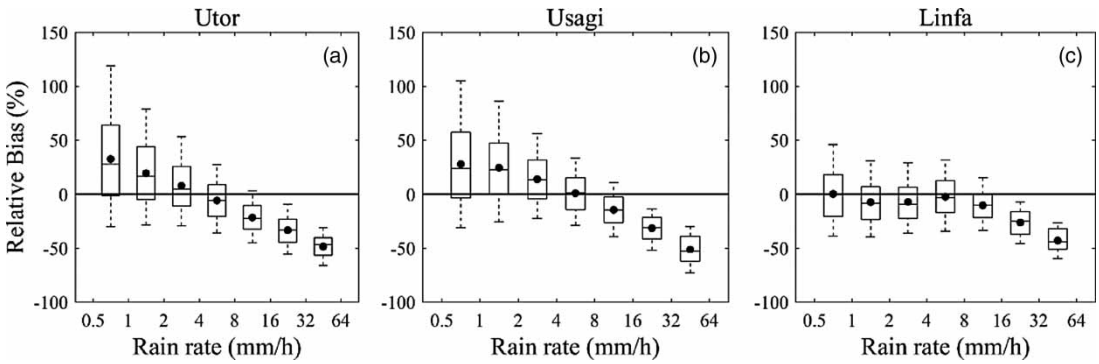

Figure 5 | RB of CMPA within different rain depth intervals for the three typhoon events. The box represents the 25 and 75% quartiles, and the line and dot within the box represent the median and mean values, respectively. The whiskers indicate the 5 and 95% percentile.

the mean FAR values vary from 0.13 to 0.31 for the seven events. FAR has an inverse pattern with POD, lower values in CMPA grids close to the typhoon center track. Meanwhile, the false count is 3–4 times of the miss count. In other words, CMPA has a relatively large FAR and small missing ratio. Moreover, the miss and false count of CMPA mainly occurs in light rain, and about 70% of miss counts are for rain hours <0.5 mm/h (Figure 6 and Figure A5 (available with the online version of this paper)).

Spatiotemporal evolutions

Accurate representation to the spatiotemporal evolutions of heavy rain is crucial in storm monitoring and flood forecasting. CMPA estimates are in agreement with the gauge observations in total rainfall and the spatiotemporal evolutions for the three types of hyetographs of the seven typhoon events (Figure 7 and Figure A6 (available with the online version of this paper)).

In the storm center (Type 1) for the Utor event, the peak rain rate occurs in the 9th–11th hours, when the Utor landed. CMPA greatly underestimates the peak rain and leads to a smaller event total rain by −15.54%, although it has a similar estimate prior to and post the peak time (Figure 7(b1)). Within the three peak hours from the 9th–11th hours, the mean rain rates from gauges were 22.7, 24.4 and 23.0 mm/h, while they were 10.5, 13.7 and 14.0 mm/h from CMPA. During the advance (Type 2) and dissipation stages (Type 3), CMPA estimates generally match the gauge observations by RB of 9.61 and 2.11% and CC of 0.95 and 0.99, respectively (Figure 7(c1) and 7(d1)). For the Usagi and Linfa events, CMPA estimates are overall in agreement with the gauge observations (Figure 7(b2)–7(d2) and 7(b3)–7(d3)). They are slightly larger than the gauge observations to Type 2 and Type 3 for the Usagi event and Type 3 for the Linfa event. There were similar patterns for the three types of hyetographs of the auxiliary four events (Table 4 and Figure A6). In other words, CMPA underestimate the intense rain and overestimate the light rain (Table 4).

SUMMARY AND REMARKS

The current satellite rainfall estimates have great potential in hydrologic and climatic applications in spite of their limitations in detecting extreme rainfall (Habib *et al.* 2009; Chen *et al.* 2013a). They usually need validation before applying in hydrologic modeling (Turk *et al.* 2008). In validation, more studies focus on the differences in rainfall amount, intensity and spatial varies between satellite estimates and ground observations, and fewer studies investigate the evolution of rainfall events (Wang *et al.* 2013b). The lately emerging CMPA product generated for continental China has higher spatial and temporal resolution (hourly and 0.1°) than the current common satellite precipitation estimates (3-hourly or daily and 0.25°) and also show better performance in quantifying extreme rainfall, but few studies have applied it to investigate the typhoon-related extreme rainfall in southern China.

This study carried out a comprehensive evaluation to the CMPA product in quantifying the typhoon-related extreme rainfall using a dense rain gauge network in Guangdong Province, China. All seven typhoon events making landfall in Guangdong Province from 2013 to 2015 were analyzed. The three typhoon storm events of Utor, Usagi and Linfa had a wider impact on the entire Guangdong

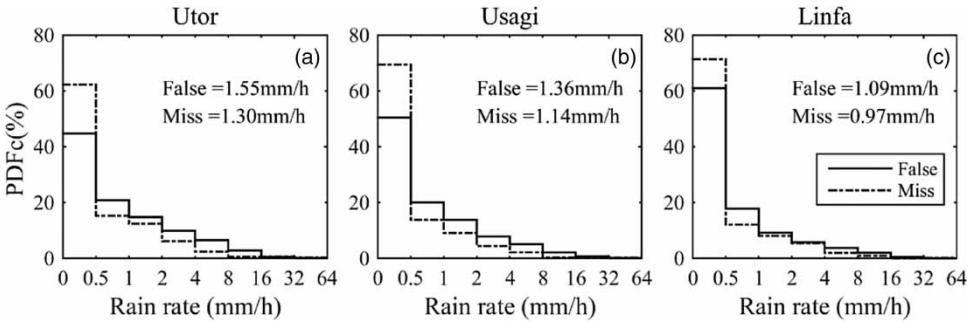

Figure 6 | Probability distribution functions by occurrence (PDFc) for the false and miss counts.

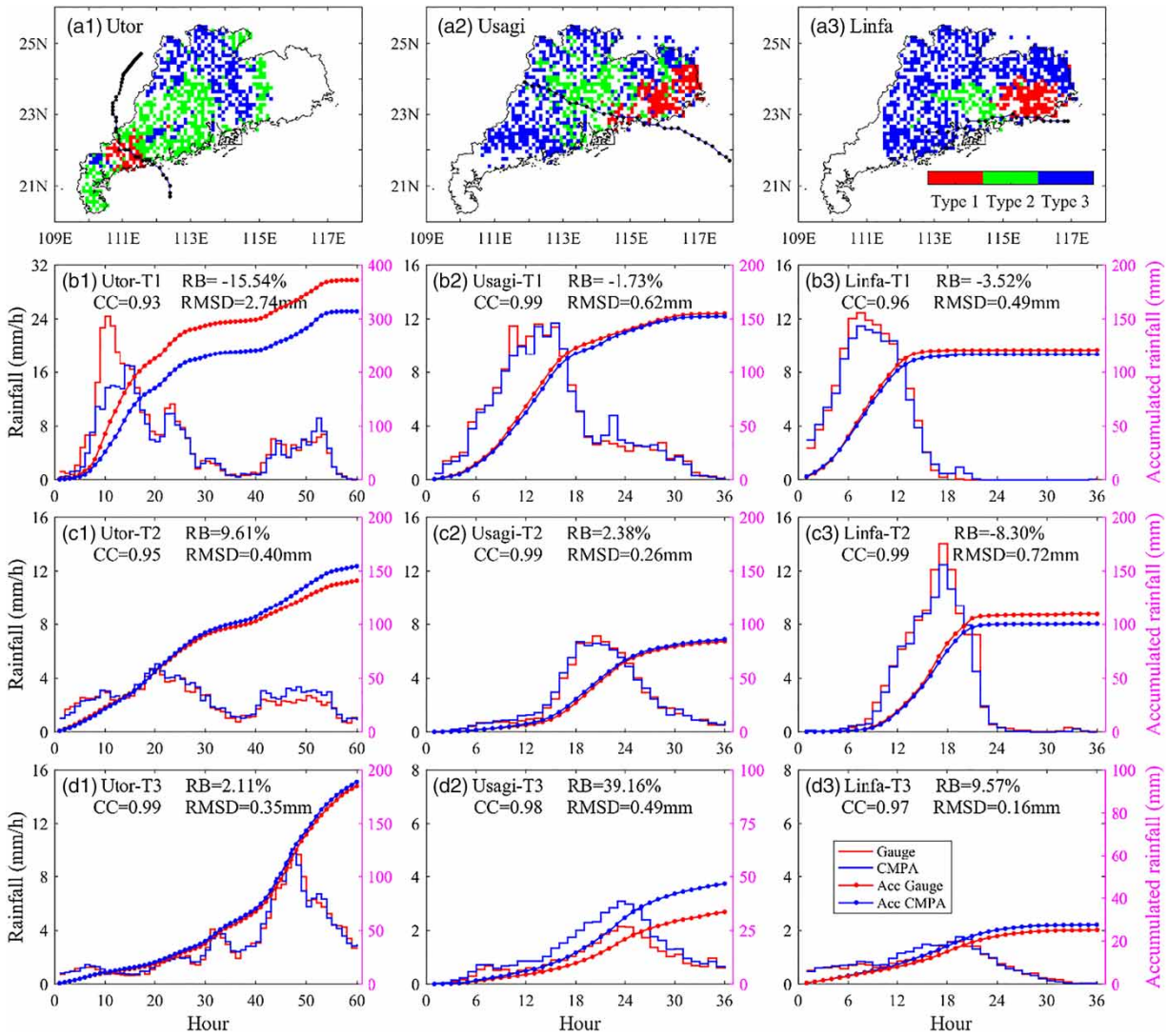

Figure 7 | (a1)–(a3) Spatial distribution of the three rain types obtained by the K-means cluster analysis from gauge observations for the Utor, Usagi and Linfa events; (b1)–(d3) hourly (stairs, left-hand vertical axis) and accumulated (lines, right-hand vertical axis) rain series from gauge and CMPA at the three clustered types of the three events.

Table 4 | RB of CMPA for the three rain types of the seven typhoon events

Event		Utor	Usagi	Linfa	Mujigae	Kalmaegi	Rammasun	Rumbia
Type 1	RB	−15.54%	−1.73%	−3.52%	−7.61%	−9.94%	−15.99%	8.08%
	P	0.005*	0.169	0.166	0.017*	0.155	0.007*	0.016*
Type 2	RB	9.61%	2.38%	8.30%	3.37%	−34.22%	−15.89%	−10.67%
	P	0.000*	0.153	0.061	0.034*	0.000*	0.001*	0.039*
Type 3	RB	2.11%	39.16%	9.57%	10.35%	10.38%	7.35%	−1.09%
	P	0.008*	0.000*	0.035*	0.000*	0.009*	0.016*	0.698

*$p < 0.05$, represents the observed difference between gauge and CMPA is significant at the 95% confidence level.

Province than the other four typhoons of Mujigae, Kalmaegi, Rammasun and Rumbia, and are illustrated in the main text. The results for the other four typhoons are provided in the auxiliary material. CMPA shows consistent performance for all seven events. The primary results are summarized below.

The hourly and event-total precipitation from CMPA is generally in agreement with gauges. CMPA captures the spatial patterns of typhoon-related rain depth. CMPA underestimates intense rain and overestimates light rain. CMPA underestimates the occurrence of light rain and heavy rain, while overestimates the occurrence of moderate rain between 2 and 16 mm/h. CMPA shows similar high POD in all seven storm events. Meanwhile, it has a relatively large FAR and small missing ratio. The miss count has a larger proportion in the low rain rate ranges, leading to a smaller mean rain rate for the miss count than that of the false count.

All gauges are further classified into three types of hyetograph, which form a spatial pattern that corresponds to the three stages of the storm evolution, the initial landfall (storm center), advance and the dissipation. Even though the performance of CMPA may vary from case to case, CMPA generally underestimates rainfall of Type 1 and overestimates rainfall of Type 3 for most events. Overall, CMPA is in agreement with the spatiotemporal evolution of gauge observation.

Why does CMPA perform slightly better along the landfall track than that farther away from the track? This might relate to the physical mechanisms and topographic effects on the typhoon-related rainfall. More studies are needed to investigate various types of typhoon-related rainfall events that land on different regions and move towards different directions.

CMPA greatly underestimates the intense rainfall larger than 16 mm/h although it provides relatively accurate information on the spatiotemporal evolution of the typhoon-related extreme rainfall. This implies that caution should be taken when applying it in hydrologic modeling for flooding forecasting. Chen *et al.* (2013a) indicated that a ground radar network performs better than satellite-based products for extreme typhoon rainfall. Further studies with a combination of the CMPA estimate and ground radars are highly recommended. Moreover, hydrologic modeling and stream flow measurements are additional validation and constraints to total rainfall volume that might not be properly represented by gauges, especially in mountainous areas.

ACKNOWLEDGEMENTS

This study was partially supported by the Natural Science Foundation of China (#41371404; #51379224; #41301419), the Water Resource Science and Technology Innovation Program of Guangdong Province (#2016-19), and the Open Foundation of the State Key Laboratory of Desert and Oasis Ecology (#Y371163), Xinjiang Institute of Ecology and Geography, Chinese Academy of Sciences. We thank all researchers and staff for providing and maintaining the meteorological data and the CMPA product from China Meteorological Administration, National Meteorological Information Center, and Water Resources Department of the Guangdong Province. Comments provided by two anonymous reviewers and the editor greatly improved this manuscript and are highly appreciated by all authors.

REFERENCES

Administration of Ocean and Fisheries of Guangdong Province (AOF) 2014 *Oceanic Disaster Bulletin of Guangdong Province in 2013*. Available from: www.gdofa.gov.cn/index.php/Catagories/view/id/174866 (accessed 27 May 2014).

Anagnostou, E. N. 2004 Overview of overland satellite rainfall estimation for hydro-meteorological applications. *Surv. Geophys.* **25** (5–6), 511–537.

Behrangi, A., Khakbaz, B., Jaw, T. C., AghaKouchak, A., Hsu, K. & Sorooshian, S. 2011 Hydrologic evaluation of satellite precipitation products over a mid-size basin. *J. Hydrol.* **397** (3), 225–237.

Chen, S., Hong, Y., Cao, Q., Kirstetter, P. E., Gourley, J. J., Qi, Y., Zhang, J., Howard, K., Hu, J. & Wang, J. 2013a Performance evaluation of radar and satellite rainfalls for Typhoon Morakot over Taiwan: are remote-sensing products ready for gauge denial scenario of extreme events? *J. Hydrol.* **506**, 4–13.

Chen, S., Hong, Y., Cao, Q., Gourley, J. J., Kirstetter, P. E., Yong, B., Tian, Y., Zhang, Z., Shen, Y., Hu, J. & Hardy, J. 2013b Similarity and difference of the two successive V6 and V7 TRMM multisatellite precipitation analysis performance over China. *J. Geophys. Res.* **118** (23), 13–60.

Chen, S., Hong, Y., Gourley, J. J., Huffman, G. J., Tian, Y., Cao, Q., Yong, B., Kirstetter, P. E., Hu, J., Hardy, J., Li, Z., Khan, S. I. &

Xue, X. 2013c Evaluation of the successive V6 and V7 TRMM multisatellite precipitation analysis over the Continental United States. *Water Resour. Res.* **49** (12), 8174–8186.

Chen, Y., Ebert, E. E., Walsh, K. J. & Davidson, N. E. 2013d Evaluation of TMPA 3B42 daily precipitation estimates of tropical cyclone rainfall over Australia. *J. Geophys. Res.* **118** (21), 11–966.

Chen, Y., Ebert, E. E., Walsh, K. J. & Davidson, N. E. 2013e Evaluation of TRMM 3B42 precipitation estimates of tropical cyclone rainfall using PACRAIN data. *J. Geophys. Res.* **118** (5), 2184–2196.

Chen, Y., Wang, H., Min, J., Huang, X. Y., Minnis, P., Zhang, R., Haggerty, J. & Palikonda, R. 2015 Variational assimilation of cloud liquid/ice water path and its impact on NWP. *J. Appl. Meteorol. Climatol.* **54** (8), 1809–1825.

Chen, S., Tian, Y., Behrangi, A., Hu, J., Hong, Y., Zhang, Z., Stepanian, P., Hu, B. & Zhang, X. 2016 Precipitation spectra analysis over China with high-resolution measurements from optimally-merged satellite/gauge observations – Part I: spatial and seasonal analysis. *IEEE J-STARS*. Doi: 10.1109/JSTARS.2016.2529003.

Dai, A., Lin, X. & Hsu, K. L. 2007 The frequency, intensity, and diurnal cycle of precipitation in surface and satellite observations over low-and mid-latitudes. *Clim. Dyn.* **29** (7–8), 727–744.

Dare, R. A., Davidson, N. E. & McBride, J. L. 2012 Tropical cyclone contribution to rainfall over Australia. *Mon. Weather Rev.* **140** (11), 3606–3619.

Dinku, T., Ceccato, P. & Connor, S. J. 2011 Challenges of satellite rainfall estimation over mountainous and arid parts of east Africa. *Int. J. Remote Sens.* **32** (21), 5965–5979.

Ebert, E. E., Janowiak, J. E. & Kidd, C. 2007 Comparison of near-real-time precipitation estimates from satellite observations and numerical models. *Bull. Am. Meteorol. Soc.* **88** (1), 47–64.

Habib, E., Henschke, A. & Adler, R. F. 2009 Evaluation of TMPA satellite-based research and real-time rainfall estimates during six tropical-related heavy rainfall events over Louisiana, USA. *Atmos. Res.* **94** (3), 373–388.

Hartigan, J. A. & Wong, M. A. 1979 Algorithm AS 136: a k-means clustering algorithm. *J. Roy Stat. Soc. C (Appl. Stat.)* **28**, 100–108.

Hong, Y., Adler, R. & Huffman, G. 2006 Evaluation of the potential of NASA multi-satellite precipitation analysis in global landslide hazard assessment. *Geophys. Res. Lett.* **33**, L22402.

Hossain, F. & Lettenmaier, D. P. 2006 Flood prediction in the future: recognizing hydrologic issues in anticipation of the Global Precipitation Measurement mission. *Water Resour. Res.* **42**, W11301.

Huang, Y., Chen, S., Cao, Q., Hong, Y., Wu, B., Huang, M., Qiao, L., Zhang, Z., Li, Z., Li, W. & Yang, X. 2013 Evaluation of version-7 TRMM multi-satellite precipitation analysis product during the Beijing extreme heavy rainfall event of 21 July 2012. *Water* **6** (1), 32–44.

Huffman, G. J., Bolvin, D. T., Nelkin, E. J., Wolff, D. B., Adler, R. F., Gu, G., Neikin, E. J., Bowman, K. P., Hong, Y., Stocker, E. F. & Wolff, D. B. 2007 The TRMM multisatellite precipitation analysis (TMPA): quasi-global, multiyear, combined-sensor precipitation estimates at fine scales. *J. Hydrometeorol.* **8** (1), 38–55.

Jiang, S., Ren, L., Hong, Y., Yong, B., Yang, X., Yuan, F. & Ma, M. 2012 Comprehensive evaluation of multi-satellite precipitation products with a dense rain gauge network and optimally merging their simulated hydrological flows using the Bayesian model averaging method. *J. Hydrol.* **452**, 213–225.

Joyce, R. J., Janowiak, J. E., Arkin, P. A. & Xie, P. 2004 CMORPH: a method that produces global precipitation estimates from passive microwave and infrared data at high spatial and temporal resolution. *J. Hydrometeorol.* **5** (3), 487–503.

Knabb, R. D., Rhome, J. R. & Brown, D. P. 2005 *Tropical cyclone report: Hurricane Katrina, 23–30 August 2005*. National Hurricane Center. Available from: www.nhc.noaa.gov/data/tcr/AL122005_Katrina.pdf (accessed 1 March 2015).

Lee, J., Kwon, H. & Kim, T. 2012 Spatio-temporal analysis of extreme precipitation regimes across South Korea and its application to regionalization. *J. Hydro-environ. Res.* **6** (2), 101–110.

Li, M. & Shao, Q. 2010 An improved statistical approach to merge satellite rainfall estimates and raingauge data. *J. Hydrol.* **385** (1), 51–64.

Li, Z., Yang, D. & Hong, Y. 2013 Multi-scale evaluation of high-resolution multi-sensor blended global precipitation products over the Yangtze River. *J. Hydrol.* **500**, 157–169.

Lonfat, M., Marks Jr, F. D. & Chen, S. S. 2004 Precipitation distribution in tropical cyclones using the Tropical Rainfall Measuring Mission (TRMM) microwave imager: a global perspective. *Mon. Weather Rev.* **132** (7), 1645–1660.

Negri, A. J., Burkardt, N., Golden, J. H., Halverson, J. B., Huffman, G. J., Larsen, M. C., McGinley, J. A., Updike, R. G., Verdin, J. P. & Wieczorek, G. F. 2005 The hurricane-flood-landslide continuum. *Bull. Am. Meteorol. Soc.* **86** (9), 1241–1247.

Peña-Arancibia, J. L., van Dijk, A. I., Renzullo, L. J. & Mulligan, M. 2013 Evaluation of precipitation estimation accuracy in reanalysis, satellite products, and an ensemble method for regions in Australia and South and East Asia. *J. Hydrometeorol.* **14** (4), 1323–1333.

Prakash, S., Mitra, A. K., Momin, I. M., Pai, D. S., Rajagopal, E. N. & Basu, S. 2015 Comparison of TMPA-3B42 versions 6 and 7 precipitation products with gauge-based data over India for the southwest monsoon period. *J. Hydrometeorol.* **16** (1), 346–362.

Prat, O. P. & Nelson, B. R. 2013 Mapping the world's tropical cyclone rainfall contribution over land using the TRMM multi-satellite precipitation analysis. *Water Resour. Res.* **49** (11), 7236–7254.

Rasmussen, K. L., Choi, S. L., Zuluaga, M. D. & Houze, R. A. 2013 TRMM precipitation bias in extreme storms in South America. *Geophys. Res. Lett.* **40** (13), 3457–3461.

Ren, F., Wu, G., Dong, W., Wang, X., Wang, Y., Ai, W. & Li, W. 2006 Changes in tropical cyclone precipitation over China. *Geophys. Res. Lett.* **33**, L20702.

Shen, Y., Zhao, P., Pan, Y. & Yu, J. 2014 A high spatiotemporal gauge-satellite merged precipitation analysis over China. *J. Geophys. Res. Atmos.* **119**, 3063–3075.

Sorooshian, S., Hsu, K. L., Gao, X., Gupta, H. V., Imam, B. & Braithwaite, D. 2000 Evaluation of PERSIANN system satellite-based estimates of tropical rainfall. *Bull. Am. Meteorol. Soc.* **81** (9), 2035–2046.

Sorooshian, S., AghaKouchak, A., Arkin, P., Eylander, J., Foufoula-Georgiou, E., Harmon, R., Hendrickx, J. M. H., Imam, B., Kuligowski, R., Skahill, B. & Skofronick-Jackson, G. 2011 Advanced concepts on remote sensing of precipitation at multiple scales. *Bull. Am. Meteorol. Soc.* **92** (10), 1353–1357.

Stampoulis, D. & Anagnostou, E. N. 2012 Evaluation of global satellite rainfall products over continental Europe. *J. Hydrometeorol.* **13** (2), 588–603.

Su, F., Hong, Y. & Lettenmaier, D. P. 2008 Evaluation of TRMM multisatellite precipitation analysis (TMPA) and its utility in hydrologic prediction in the La Plata Basin. *J. Hydrometeorol.* **9** (4), 622–640.

Tian, Y., Peters-Lidard, C. D., Choudhury, B. J. & Garcia, M. 2007 Multitemporal analysis of TRMM-based satellite precipitation products for land data assimilation applications. *J. Hydrometeorol.* **8** (6), 1165–1183.

Turk, F. J. & Miller, S. D. 2005 Toward improved characterization of remotely sensed precipitation regimes with MODIS/AMSR-E blended data techniques. *IEEE Trans. Geosci. Remote Sens.* **43** (5), 1059–1069.

Turk, F. J., Arkin, P., Sapiano, M. R. & Ebert, E. E. 2008 Evaluating high-resolution precipitation products. *Bull. Am. Meteorol. Soc.* **89** (12), 1911–1916.

Van Nguyen, H. & Chen, Y. L. 2011 High-resolution initialization and simulations of Typhoon Morakot (2009). *Mon. Weather Rev.* **139** (5), 1463–1491.

Wang, X., Xie, H., Sharif, H. & Zeitler, J. 2008 Validating NEXRAD MPE and Stage III precipitation products for uniform rainfall on the Upper Guadalupe River Basin of the Texas Hill Country. *J. Hydrol.* **348** (1), 73–86.

Wang, P., Wu, W., Zhu, B. & Wei, Y. 2013a Examining the impact factors of energy-related CO_2 emissions using the STIRPAT model in Guangdong Province, China. *Appl. Energy* **106**, 65–71.

Wang, X., Xie, H., Mazari, N., Zeitler, J., Sharif, H. & Hammond, W. 2013b Evaluation of a near-real time NEXRAD DSP product in evolution of heavy rain events on the Upper Guadalupe River Basin, Texas. *J. Hydroinform.* **15** (2), 464–485.

Wang, D., Jiang, P., Wang, G. & Wang, D. S. 2015 Urban extent enhances extreme precipitation over the Pearl River Delta, China. *Atmos. Sci. Lett.* **16**, 310–317.

Wu, H., Adler, R. F., Hong, Y., Tian, Y. & Policelli, F. 2012 Evaluation of global flood detection using satellite-based rainfall and a hydrologic model. *J. Hydrometeorol.* **13** (4), 1268–1284.

Yang, L., Scheffran, J., Qin, H. & You, Q. 2015 Climate-related flood risks and urban responses in the Pearl River Delta, China. *Reg. Environ. Change* **15** (2), 379–391.

Yin, S., Wang, Y., Xie, Y. & Liu, A. 2014 Characteristics of intra-storm temporal pattern over China. *Shuikexue Jinzhan/Adv. Water Sci.* **25** (5), 617–624 (in Chinese).

Yong, B., Ren, L. L., Hong, Y., Wang, J. H., Gourley, J. J., Jiang, S. H., Chen, X. & Wang, W. 2010 Hydrologic evaluation of multisatellite precipitation analysis standard precipitation products in basins beyond its inclined latitude band: a case study in Laohahe basin, China. *Water Resour. Res.* **46**, W07542.

Yong, B., Chen, B., Gourley, J. J., Ren, L., Hong, Y., Chen, X., Wang, W., Chen, S. & Gong, L. 2014 Intercomparison of the Version-6 and Version-7 TMPA precipitation products over high and low latitudes basins with independent gauge networks: is the newer version better in both real-time and post-real-time analysis for water resources and hydrologic extremes? *J. Hydrol.* **508**, 77–87.

Yu, M. & Liu, Y. 2015 The possible impact of urbanization on a heavy rainfall event in Beijing. *J. Geophys. Res.* **120** (16), 8132–8143.

Yu, Z., Yu, H., Chen, P., Qian, C. & Yue, C. 2009 Verification of tropical cyclone-related satellite precipitation estimates in mainland China. *J. Appl. Meteorol. Climatol.* **48** (11), 2227–2241.

Yu, H., Chen, B., Chiu, C., Lu, M. & Tung, C. 2014 Analysis of space–time patterns of rainfall events during 1996–2008 in Yilan County (Taiwan). *Stoch. Environ. Res. Risk A* **29** (3), 929–945.

Zeng, W., Lao, X., Rutherford, S., Xu, Y., Xu, X., Lin, H., Liu, T., Luo, Y., Xiao, J., Hu, M., Chu, C. & Ma, W. 2014 The effect of heat waves on mortality and effect modifiers in four communities of Guangdong Province, China. *Sci. Total Environ.* **482**, 214–221.

Zhang, J., Howard, K., Langston, C., Vasiloff, S., Kaney, B., Arthur, A., Van Cooten, S., Kelleher, K., Kitzmiller, D., Ding, F., Seo, D. J., Wells, E. & Dempsey, C. 2011a National Mosaic and Multi-Sensor QPE (NMQ) system: description, results, and future plans. *Bull. Am. Meteorol. Soc.* **92** (10), 1321–1338.

Zhang, Q., Zhang, W., Chen, Y. D. & Jiang, T. 2011b Flood, drought and typhoon disasters during the last half-century in the Guangdong Province, China. *Nat. Hazards* **57** (2), 267–278.

Zhou, T., Yu, R., Chen, H., Dai, A. & Pan, Y. 2008 Summer precipitation frequency, intensity, and diurnal cycle over China: a comparison of satellite data with rain gauge observations. *J. Clim.* **21**, 3997–4010.

First received 21 December 2015; accepted in revised form 14 June 2016. Available online 30 July 2016